Magazine of Civil Engineering

ISSN 2712-8172

journal homepage: http://engstroy.spbstu.ru/

Research article

UDC 691.5

DOI: 10.34910/MCE.122.9

Performance of aluminium shaving waste and silica fume blended mortar

M.O. Yusuf ✉

Department of Civil Engineering, College of Engineering, University of Hafr Al Batin, Hafr Albatin, Saudi Arabia

✉ moruf@uhb.edu.sa, moruff@gmail.com

Keywords: compressive strength, hydration, thermal conductivity, supplementary cementitious materials, silica fume, microstructure

Abstract. This study investigates the impact of aluminium shaving waste (ASW or A_x: 0.0, 1.0, 1.5, 2 wt%) on the silica fume (SF or S_y: 0-10 %) blended ordinary Portland cement (OPC or $C_{88\text{-}100\%}$) mortar. The sample was designated as $C_{100\text{-}x\text{-}y}S_yA_x$ and the evaluations were done through their performances in terms of workability, compressive strength, thermal residual strength and microstructural characteristics in comparison with the OPC only mortar ($C_{100}S_0A_0$). The increase in ASW/SF ratio enhanced the workability of SF blended ($C_{90\text{-}x}S_{10}A_x$). The unit weight of mortar reduced with increase in ASW/SF ratio so that 19.7 % was lost with the incorporation of 2 % of ASW. ASW induced effervescence of hydrogen gas in the fresh sample thereby leading to unit-weight reduction. The inclusion of 1 % ASW in ternary blending gave the optimum performances of 28-day strength (53.8 MPa) and residual thermal (300 °C, 1 h) strength of 56 MPa that had a comparable value to OPC mortar (55 MPa) unexposed to the thermal treatment. ASW also caused thermal stability in SF-ASW blended mortar as addition of 0.5, 1.5 and 2 % ASW caused 33.8, 15.6 and 33.4 % loss in 28-day strengths, respectively, while the least was observed in 1 % ASW sample with the loss of 8.8 %. Finally, ASW enhanced weight reduction (at 300 °C for 1 h) as the unit weight reduced by 1.75, 4.89, 3.30 and 1.86 % in $C_{89.5}S_{10}A_{0.5}$, $C_{89}S_{10}A_1$, $C_{88.5}S_{10}A_{1.5}$ and $C_{88}S_{10}A_2$, respectively, in comparison with $C_{100}S_0A_0$. Mayenite and muscovite could be formed as products when ASW is used as supplementary materials in silica fume blended mortar production.

Acknowledgements: The authors would like to appreciate the remarks of the anonymous reviewer who has greatly improved the manuscript. The continuous support of University of Hafr Al Batin is appreciated.

Citation: Yusuf, M.O. Performance of aluminium shaving waste and silica fume blended mortar. Magazine of Civil Engineering. 2023. Article no. 12209. DOI: 10.34910/MCE.122.9

1. Introduction

Production of ordinary Portland cement that is used as a binder in mortar and concrete involves breaking down limestone with high amount of energy; this leads to proliferation of carbon dioxide, which causes global warming by damaging the ozone layer. The use of supplementary cementitious (SCMs) materials such as pozzolanic (fly ash, palm oil fuel ash, metakaolin and silica fume) and and other hydraulic materials such as ground granulated blast furnace slag (GGBFS) have been adopted by several researchers towards achieving cost efficiency and sustainable environment. Utilization of solid wastes has significantly reduced the volume of landfills in our environment. This solid waste could emanate from agricultural and industrial wastes. The industrial wastes such as iron-filling, cement kiln dust, and glass wastes have been recently reported to have contributed significantly to both fresh and hard properties of pastes, mortars, and concrete [1].

One of these industrial wastes is aluminium shaving waste (ASW), which is obtained through aluminium frames reshaping process by using lathe or turret mills. Aluminum (Al) is a non-ferrous metal reported to be light, conductive, and corrosion resistant. It can attract oxygen, and has viable potential for engineering applications since the end of the 19th century [2]. International Aluminium Institute (IAI) reported 5,273 thousand metric tons of aluminium production as of February 2023, while the main aluminium scraps came from construction and automobile industries [3]. The carbon dioxide equivalent (CO_2e) owing to recycling of aluminium waste amounted to 22 million metric tons with substantial part obtained from the thermal energy source. It becomes imperative for civil engineers to develop a technique towards ensuring some aluminium wastes are safely used in concrete and mortar production.

In this regard, Ofuyatan et al. [4] used varied aluminium shaving waste (ASW) in volume of 1–2 % and studied its contribution to the bond strength of laterized concrete beams with a view to minimize industrial waste. They reported that ASW decreased compressive strength but increased bond strength of reinforcement with concrete. Lower diameter bar of 16 mm performed better than a 20 mm diameter bar. Gulmez [5] also used 1-4 wt% of ASW as fine aggregate with a noticeable decrease in bulk density while flexural strength and transport characteristics increased due to more porosity of the matrix. Tang Van et al. [6] also used the combination of 30 % fly ash (FA) and ASW to achieve production of aerated concrete with lower density and modulus of elasticity, but higher porosity. The 28-day compressive strength of 52.7 MPa was achieved due to silica and alumina interaction [7]. Shabbar et al. [8] also reported inclusion of 0.5 to 1 wt% of aluminium (Al) powder decreased the elastic modulus and density of concrete. Moghaddam et al. [9] also asserted that Al nanoparticles can react with portlandite to produce aluminosilicate-hydrate gel while its synergy with glass waste could reduce the absorption of the samples.

Furthermore, Kuziak et al. [10] investigated alumina powder in two different types of cement (CEM 1 and III) and discovered that the rate of hydrogen gas effervescence in Al-blended binder depends on the amount of portlandite that accompanied hydration process as this could have a negative effect on strength [11]. Moreover, incorporation of 1 wt% alumina into slag blended cement (CEM III) could cause cracks due to the interconnected pore formations. In addition, an introduction of alumina into a lime-dominated binder could also have a negative impact on strength and density of the binder, especially in an aerated concrete. Similarly, Ramamurthy et al. [12–13] indicated that lime/cement ratio plays a significant role for strength and density. Autoclave curing of aerated mortar with high aluminium content (0.6–0.8 %) could lead to coalescence of discreet pores thereby causing minimization of pore total surface areas, which in turn may result in a decrease in the strength of the products [14].

Narayanan et al. [15] asserted that curing methods for aerated concrete play a significant role in the microstructural properties, chemical compositions, and density of aerated concrete with the incorporated aluminium powder. Sabapathy et al. [3] incorporated 0.5–2 vol% aluminium fiber in concrete samples with a view to enhance the compressive and split tensile strengths at a water/binder ratio of 0.6 (M20), 0.45 (M30) and 0.4 (M40). The optimum fiber content for compressive strength and split tensile strength were 0.5 % and 2 %, respectively. Elinwa and Mbadike [16] also asserted that large aluminium waste (AW) content within 5–40 % in concrete can be used as a retarder with 10 % being the optimum for compressive and flexural strengths.

Moreover, Azarhomayun et al. [17] used Al powder to reduce free shrinkage and crack width in concrete but also increase the restrained drying shrinkage by 18 %. The presence of excessive AW embedded in concrete could cause cracks due to pressure exerted by Al corrosion products rather than effervescence of hydrogen [18]. Faez et. al. [19] found that alumina nanoparticles (2.5 %) blended with silica fume (10 % SF) enhanced 90-day compressive and split tensile strengths by 86 % and 47 %, respectively. Besides, adding aluminium nanoparticles with SF could reduce water absorption of concrete samples.

Despite the plethora of the studies on the incorporation of aluminium waste in aerated an lightweight concrete, little is known of the impact of the synergy between Al shaving waste (ASW) and SF in terms of strength, nature of the product, microstructure, and thermal performance of their combination in ternary blended mortar that comprises SF, ASW and OPC. It is expected that utilization of these solid wastes will reduce the amount of solid waste in landfill on one hand while it will also have a significant impact on the mechanical and microstructural properties of the final product.

This study is aimed at providing necessary information with a view to bridging the gap needed for the deeper understanding of the synergy of ASW and SF in mortar production. It also makes alternative materials available for repair and rehabilitation of concrete structure while ensuring a safe environment by limiting ASW in dumpsites or landfills.

2. Methods and Materials

2.1. Materials

2.1.1 Aluminium shaving waste

Aluminium shaving waste (ASW) as shown in Fig. 1 is a by-product from an aluminium frame processing factory obtained through grinding and cutting by lathe machine (Fig. 1). The oxide composition mainly comprises alumina with traces of Fe_2O_3, CaO, MgO, SrO and TiO_2 as shown in Table 1. Fig. 2 shows the X-ray diffractogram of the ASW.

Figure 1. Aluminium shaving.

Table 1. Oxides composition of the raw materials.

Oxides	Silica fume	Cement	Aluminium shaving waste
SiO_2	95.85	20.17	-
Al_2O_3	0.26	5.58	99.10
Fe_2O_3	0.05	2.86	0.16
CaO	0.21	63.51	0.09
MgO	0.45	3.15	0.58
Na_2O	0.40	0.12	-
K_2O	1.22	0.57	-
SO_3	1.00	2.56	-
SrO	-	-	0.01
TiO_2	-	-	0.04
$SiO_2+Al_2O_3+Fe_2O_3$	96.16	28.61	99.26
Specific gravity (water)	2.25	3.15	1.18
LOI (%)	2.48	2.80	20.0

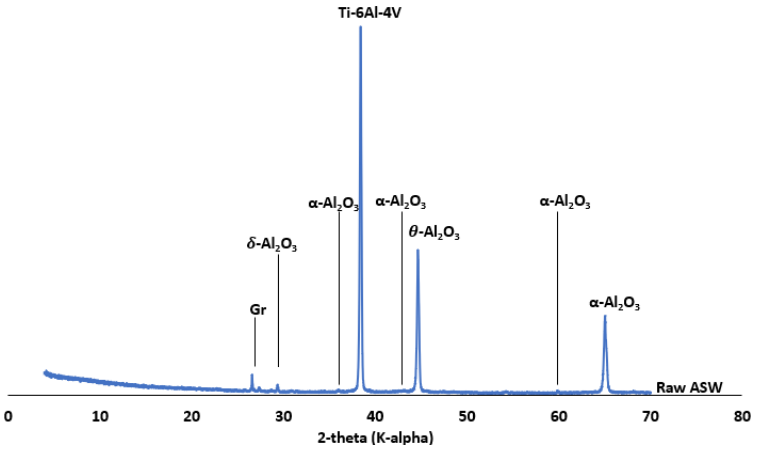

Figure 2. X-ray diffraction of aluminium shaving waste powder.

2.1.2 Cement

Type 1 ordinary Portland cement (OPC) was prepared in accordance with ASTM C 150 [20] with specific gravity (by water) of 3.15 and its oxides composition as shown in Table 1. The surface area and loss on ignition (LOI) are 329.5 m^2/kg and 2.8 %, respectively, while SiO_2, Al_2O_3, and Fe_2O_3 were summed up to 28.61 %. Fig. 3 shows the chemical compounds present in OPC as used in the study.

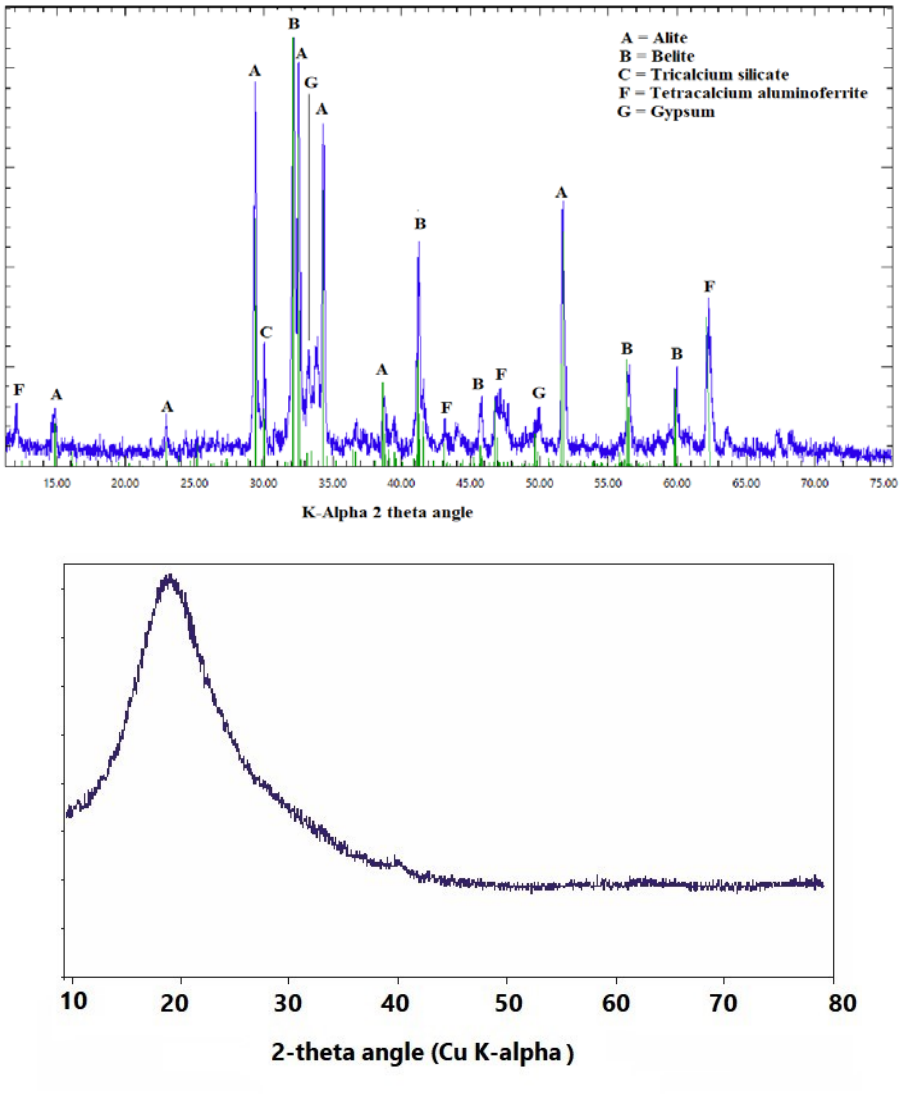

Figure 3. XRD diffractogram of ordinary Portland cement (topmost) and the silica fume (bottom).

2.1.3 Silica fume

Silica fume (SF) is commercially obtained with a relative density, LOI and surface area of 2.25, 2.48 %, and 22,800 m^2/kg, respectively with the sum of SiO_2, Al_2O_3, and Fe_2O_3 being 96.2 % as shown in Table 1, while Fig. 3 (bottom) shows its XRD diffractogram.

2.1.4. Fine aggregates

Natural sand in saturated surface dry (SSD) conditions whose moisture content and absorption were 3.43 and 6.14 %, respectively. The fine aggregate passes through a 2.36 mm sieve (No. 8) in accordance with ASTM C 157/C 157M – 08 [21]. The fineness modulus and relative density (water) were 2.8 and 2.71, respectively.

2.1.5 Superplasticizer

The superplasticizer (Glenium 51®) was used to enhance the consistency of the mixture. It is polycarboxylic ether and the proportion used was 1 % of the total binder (OPC, SF, and ASW).

2.2. Experimental tests

2.2.1 Workability

The consistency of the mortar sample was tested by using flow table in accordance with ASTM C 1437-20 [22].

2.2.2. Compressive strength

The compressive strength was determined by using 50 mm cubic samples, room-cured and subsequently exposed to thermal (300 °C for 1 h) treatment, in accordance with ASTM C 109 [23]. The testing was done by a universal testing machine at the ages 7, 14, and 28 days with the loading rate of 0.9 kN/s. The compressive strength was taken as the average of the three samples.

2.2.3 Unit weight of samples

The unit weight (KN/m^3) of samples was determined by measuring the mass (kg) of the samples at specific days, multiplying it by the acceleration due to gravity (10 m/s^2) and dividing it by the volume of the sample (125×10^{-6} m^3).

2.3 Characterization and morphology of the samples

XRD Bruker apparatus model d2-Phaser with CuKa radiation (40 kV, 40 mA) was used to determine the compound present in the product of ASW-SF blended mortar with a scan speed of 2.5°/min and continuous scanning with 2-theta angle range of 10–80°. The raw and post thermally treated ASW powder were tested to understand its phase transformation. Fourier transform infrared (FTIR) spectroscopy measurements of ASW-SF paste were conducted by using Perkin Elmer 880 spectrometer. The scanning electron microscopy and energy dispersive spectroscopy (SEM+EDS) instrument model 5800 LV manufactured by JEOL was used at an accelerating voltage of 20 kV for the microstructural characterizations and elemental compositions of the paste samples.

2.3. Sample preparation

2.4.1 Sample designation

The samples were composed of OPC (88-100%), ASW (0, 0.5, 1, 2 %) and 10% SF. The sample was designated as $C_{OPC\%}S_{SF\%}A_{Al\%}$, and thus a sample that contained 88 % OPC, 10 % SF and 2 % ASW, was designated as $C_{88}S_{10}A_2$, while the control was taken as the sample that contained OPC only, labelled as $C_{100}S_0A_0$.

2.4.2 Mix design

Mix design of the sample is given in Table 2 with the total binder of 350 kg/m^3 such that the water/binder ratio is 0.4. The binder/sand ratio was maintained at 2.5 while ASW/binder ratio varied from 0 to 2 % at the interval of 0.5.

2.4.3 Mixing procedure

Mixing was done in the following way. OPC, SF, and ASW were mixed dry for 3 mins. Half of the needed water together with the superplasticizer was poured into the mixer and then mixed for 3 mins to form a grout. Fine aggregates were then added and mixed for additional 2 mins before adding the other half of the water mixed with superplasticizer for 3 mins to achieve a homogenous mixture. Steel moulds with the dimensions of 50×50×50 mm were then oiled for easy demoulding, and to receive the fresh mortar. The cast specimens were left in the moulds for 24 h before being demoulded and then placed in the curing tank for a specified number of days (7, 14, 21 and 28 days) before being tested for compressive strength at a loading rate of 0.9 kN/s.

Table 2. Mixture proportion of aluminium shaving waste blended mortar.

Designation	Cement kg/m^3	Silica fume kg/m^3	Aluminium shaving waste kg/m^3	Sand kg/m^3	water kg/m^3	SP kg/m^3
$C_{100}S_0A_0$	350.00	0	0.00	875	140	3.5
$C_{90}S_{10}A_0$	315.00	35	0.00	875	140	3.5
$C_{89.5}S_{10}A_{0.5}$	313.25	35	1.75	875	140	3.5
$C_{89}S_{10}A_1$	311.50	35	3.50	875	140	3.5
$C_{88.5}S_{10}A_{1.5}$	309.75	35	5.25	875	140	3.5
$C_{88}S_{10}A_2$	308.00	35	7.00	875	140	3.5

3. Results and Discussions

3.1. Oxide compositions and compound in aluminium shaving waste

Table 1 shows the oxide composition of aluminium shaving waste, and it is mainly composed of 99 % alumina with traces of calcium, magnesium, iron, titanium, and strontium oxides. The ASW is very stable at thermal exposure to the tune of 1000 °C; the loss on ignition (LOI) was 20 % while the specific gravity (water) is 1.18. The presence of graphite in the X-ray diffraction (XRD) diffractogram as shown in Fig. 2 increased the value of LOI recorded while the observable main crystalline phases in ASW are graphite (COD#1200018), calcite (COD#1010962), titanium (COD# 9011600), and α-alumina (α-Al_2O_3) (COD#1533936).

The crystalline phases include graphite and Ti-6Al-4V (TC4) at the 2-theta angle of 27 °C and 39 °C, respectively. Upon subjecting it to 1000 °C as shown in Fig. 4, graphite and T4 phase disappeared thereby leading to the formation of more crystalline phases of κ-Al_2O_3 and α-Al_2O_3 and spinel (COD#9001364). This resulted in lowering of the amorphous content of ASW [24]. It has been reported that δ- and γ-alumina could transform into more crystalline phases of α- and θ-alumina with low surface area [24]. Comparing Figs. 2-4 makes it apparent that subjecting ASW to elevated temperatures transforms it into more crystalline phase.

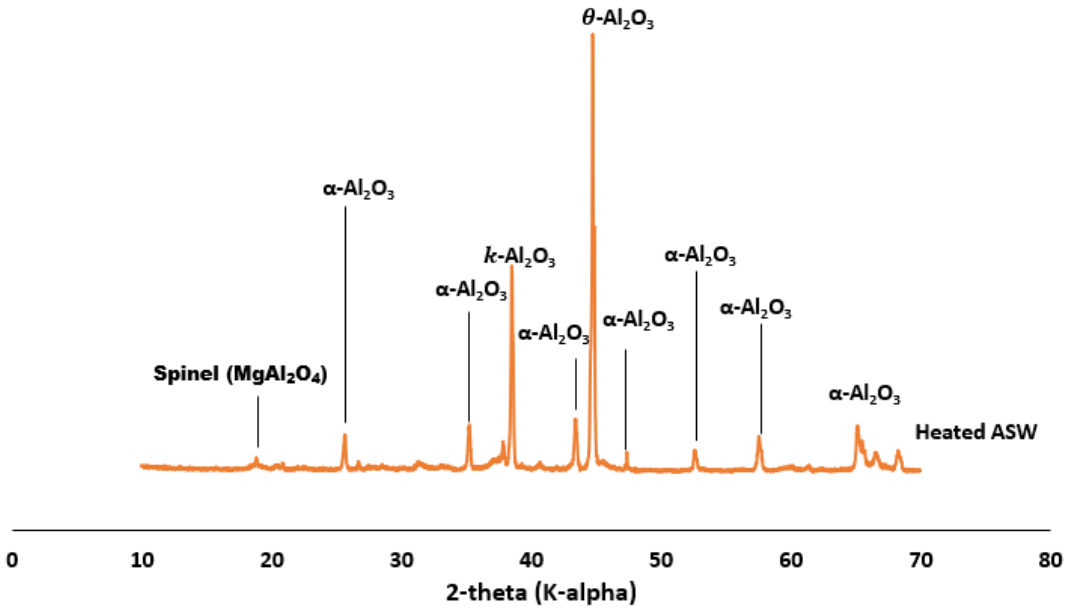

Figure 4. Phases of compounds formed upon subjecting ASW to 1000 °C.

3.2. Workability of the mortar

From Fig. 5, OPC mortar ($C_{100}S_0A_0$) had a flow diameter of 225 mm, which decreased by 20 % upon adding SF. The incorporation of 0.5 % ASW to OPC mortar ($C_{99.5}S_0A_{0.5}$) increased the consistency by 11.11 % whereas that of 10 % SF-ASW blended mortar reduced it by 6, 4.8 and 2.0 %, upon adding 0.5, 1, and 1.5 % ASW, respectively. As ASW became 2 %, no change was observed in the consistency of the mortar. Therefore, flowability of ASW-SF blended mortar was increasing with ASW/SF ratio. With reference to $C_{100}S_0A_0$, the consistency of 10 % SF–ASW blended mortar increased by 4.4 %, 5.8 %, 8.9 %, and 11.11 % as ASW was 0.5, 1, 1.5 and 2 %, respectively.

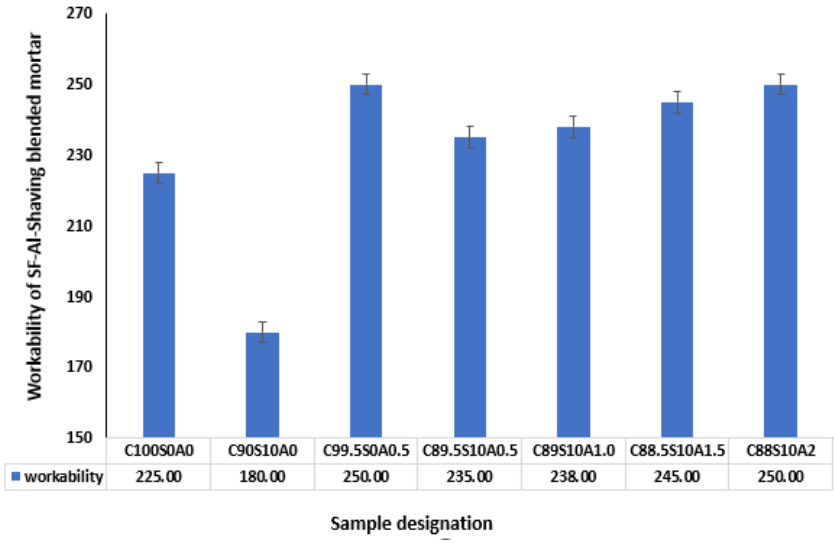

Figure 5. Consistency of SF-ASW blended mortar.

Furthermore, by comparing 10%SF–x%ASW blended mortar with SF-OPC mortar (no ASW), the workability increased by to 30.56, 32.22, 36.11 and 38.89 % with ASW content (x) of 0.5, 1, 1.5 and 2 %, respectively. This suggests that incorporation of ASW enhanced the flowability of SF-OPC mortar as shown in Fig. 5. The increase in the consistency of the mortar could be due to the reaction of portlandite with Al [25, 26] as shown in Eq. (1) thereby leading to the formation of entrapped hydrogen gas (Fig. 6) that formed a spherical ball within the matrix.

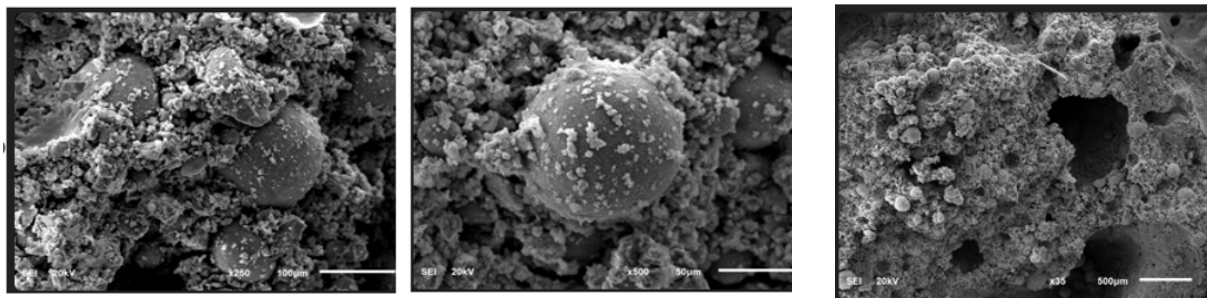

Figure 6. Formation of spherical bubble due to formation of hydrogen gas.

The presence of Al also enhances the formation of ettringite $Ca_6Al_2(SO_4)_3(OH)_{12}\cdot 26H_2O$ due to its interaction with portlandite and water to form calcium aluminate hydroxide and liberation of hydrogen gas as shown in Eq. (1):

$$2Al + 3Ca(OH)_2 + 6H_2O \rightarrow 3CaO.Al_2O_3.6H_2O + 3H_2. \quad (1)$$

The formation of hydrogen gas led to internal bubble formation that later caused pore formation due to the effervescence of the gas as shown in Fig. 6. This reaction becomes spontaneous due to formation and oxidation of $Al(OH)_3$ that accompanies dissolution of OPC that leads to the formation of hydroxyl ions.

The presence of hydroxyl ion oxidizes $Al(OH)_3$ to become $Al(OH)_4$ ion thereby making ASW undergo continuous corrosion as shown in Eq. (2) [27]. The corrosion of ASW and effervescence of hydrogen gas led to loss of fluidity of the mortar. This phenomenon depends on the concentration and quantity of ASW present in the mixture.

$$OH^- + Al(OH)_3 \rightleftharpoons Al(OH)_4^-. \quad (2)$$

At lower ASW incorporation of 0.5 % without the presence of SF, the workability increases due to attachment of Al to OH ions thereby causing disintegration of hydrogen bonding within the ettringite formation. The presence of ASW led to formation of Al-OH thereby decreasing OH^-/Al ratio, which induces ionic repulsion within ettringite. This explains why $C_{100}S_{10}A_{0.5}$ has better consistency (250 mm) compared to $C_{100}S_0A_0$ (225 mm) as shown in Fig. 5. Upon introducing SF into the mixture, silicic acid ($Si(OH)_4$) would be formed thereby reducing the pH of the mixture. The presence of SF-ASW reduces the viscosity of the mixture. This is further enhanced by the fineness of SF.

3.3. Unit weight of samples

Inclusion of the ASW and SF decreased the unit weight of the blended and OPC mortar due the specific gravity and escape of hydrogen from the pores within the matrix. With reference to $C_{100}S_0A_0$ (Fig. 7), the unit weight of OPC mortar increased from by 1.65 % within the 1 to 7 days, while it was 2.1 % in 10%SF-OPC mortar. The addition of 0.5, 1, and 1.5 % ASW made the increment to be 0.68 %, 3.93 %, and 4.33 %, respectively in 10%SF+ASW blended mortar. Upon increasing the ASW to 2 %, there was a decrease in unit weight by 5.42 %. Within the interval of 7-14 days, the increment became 0.24 % in $C_{100}S_{10}A_0$ but increased to 0.68 % in $C_{90}S_{10}A_0$. Inclusion of 0.5 % ASW led to an increase in the unit weight by 0.68 %, but reduced by 2.7 %, 2.8 %, and 5.9 %, upon adding 1, 1.5, and 2 % ASW, respectively. Within the interval of 14 to 28 days, the unit weight of OPC mortar and SF-blended mortar increased by 0.89 % and 0.34 %, respectively. The unit weight in 10%SF+ASW reduced by 0.08, 0.35, 1.06 and 0.64 % in $C_{89.5}S_{10}A_{0.5}$, $C_{89}S_{10}A_1$, $C_{88.5}S_{10}A_{1.5}$ and $C_{88}S_{10}A_2$, respectively.

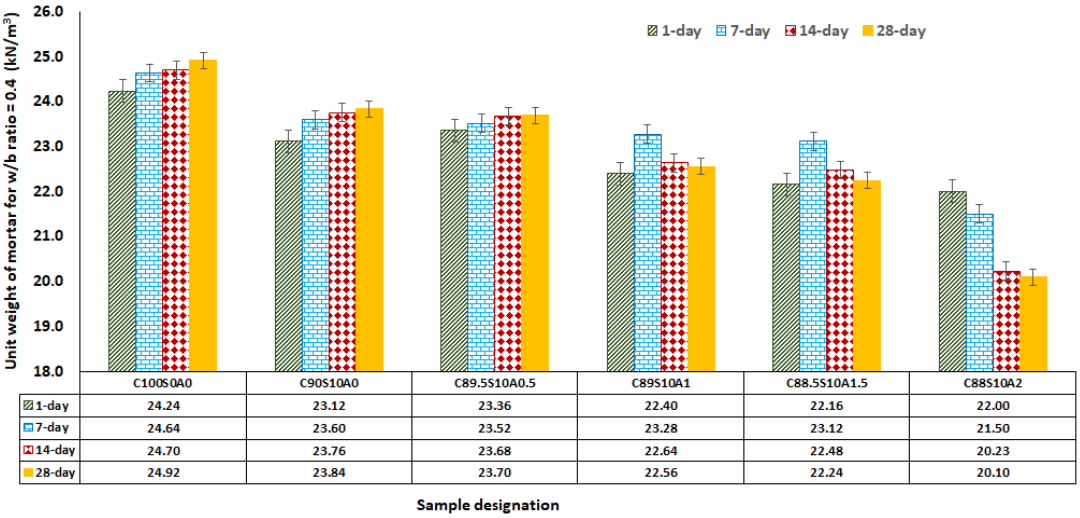

	C100S0A0	C90S10A0	C89.5S10A0.5	C89S10A1	C88.5S10A1.5	C88S10A2
1-day	24.24	23.12	23.36	22.40	22.16	22.00
7-day	24.64	23.60	23.52	23.28	23.12	21.50
14-day	24.70	23.76	23.68	22.64	22.48	20.23
28-day	24.92	23.84	23.70	22.56	22.24	20.10

Figure 7. Change in unit weight of SF-ASW blended mortar with age.

Fig. 8 shows the OPC samples exposed to thermal (300 °C) treatment lost 13.0 % of unit weight, and upon incorporating 10%SF and ASW, the loss in unit weight reduced to 12.0 %, 4.2 %, 4.3 % in $C_{89.5}S_{10}A_{0.5}$, $C_{89}S_{10}A_1$, and $C_{88.5}S_{10}A_{1.5}$, respectively, while a 4.4 % increment in unit weight was recorded in $C_{88}S_{10}A_2$. The loss in unit weight was due to removal of water from the capillary of the matrix and the disappearance of the embedded hydrogen gas. By comparing the unit weight of OPC sample ($C_{100}S_0A_0$) subjected to 300 °C, inclusion of ASW in SF blended mortar increased post-thermal unit weight by 1.75, 4.89, 3.30 and 1.86 % in $C_{89.5}S_{10}A_{0.5}$, $C_{89}S_{10}A_1$, $C_{88.5}S_{10}A_{1.5}$ and $C_{88}S_{10}A_2$, respectively.

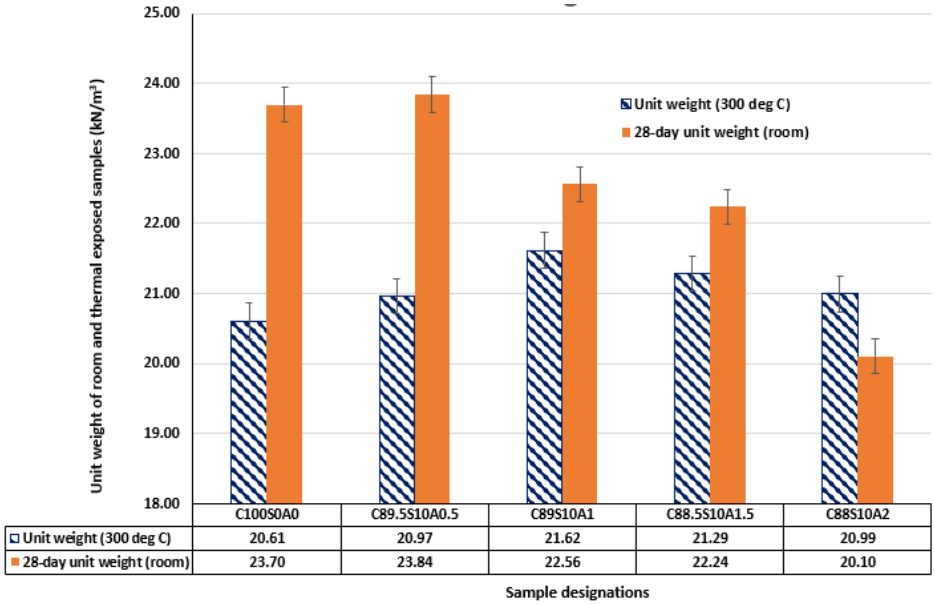

	C100S0A0	C89.5S10A0.5	C89S10A1	C88.5S10A1.5	C88S10A2
Unit weight (300 deg C)	20.61	20.97	21.62	21.29	20.99
28-day unit weight (room)	23.70	23.84	22.56	22.24	20.10

Figure 8. Unit weight of samples due to room curing and thermal treatment.

3.4. Compressive strength of ASW-SF blended mortar

As seen in Fig. 9, the presence of ASW without SF ($C_{99.5}S_0A_{0.5}$) reduced the 7, 14 and 28-day strengths by 23.3, 8.7 and 16.7 %, respectively, in comparison with OPC mortar ($C_{100}S_0A_0$). Upon adding only SF into OPC mortar ($C_{90}S_{10}A_0$), the 7 and 14-day strengths reduced by 14.2 and 14.6 %, respectively, while its 28-day strength increased by 7.1 % due to secondary hydration process of pozzolanic material in the matrix.

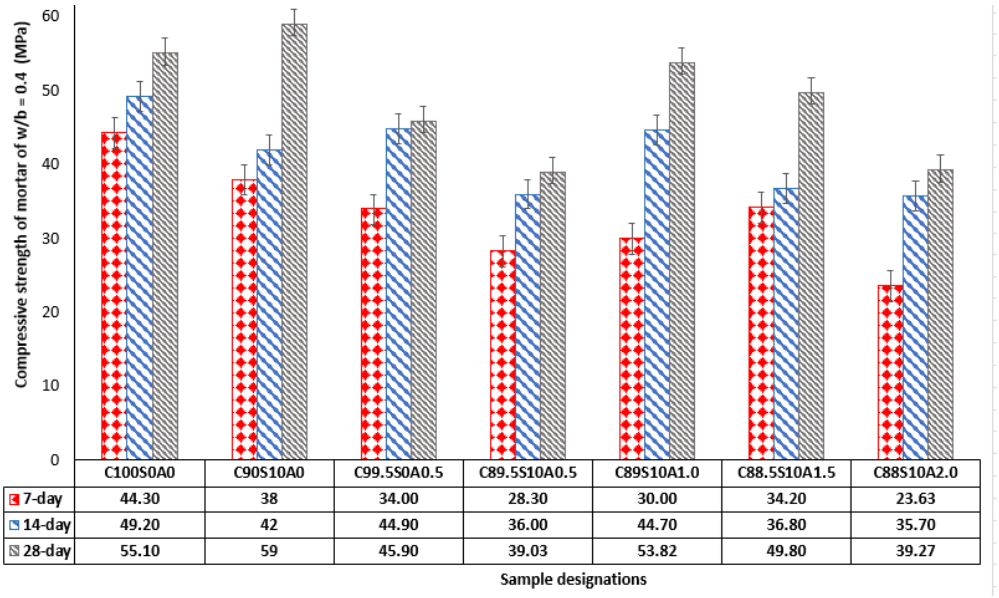

Figure 9. Compressive strength of ASW-SF blended mortar.

However, blending 0.5 % ASW with SF ($C_{89.5}S_{10}A_{0.5}$) further reduced the 7, 14 and 28-day strengths in comparison with $C_{100}S_0A_0$ by 36.1, 26.8 and 29.2%, respectively. In $C_{89}S_{10}A_1$, the reductions in strengths compared to $C_{100}S_0A_0$ were 32.3, 9.1 and 2.3 %, respectively. Increasing the ASW to 1.5 % and 2 % caused further reduction of 7, 14 and 28-day strengths to 22.8, 25.2 and 9.6% ($C_{88.5}S_{10}A_{1.5}$), and 46.7, 27.4 and 28.7 %, respectively ($C_{88}S_{10}A_2$) compared to $C_{100}S_0A_0$. Besides, the rate of strength gain in $C_{100}S_0A_0$ increased from 7 to 14 days and from 14 to 28 days by 11.1 and 12 %, respectively. For SF+OPC mortar, the rate from 7 to 14 days reduced by 4.8 % and 31.3 % in $C_{90}S_{10}A_0$ and $C_{88.5}S_{10}A_{1.5}$, respectively while the strength increased by 189.8, 146, 343 and 361.8% in $C_{99.5}S_0A_{0.5}$, $C_{89.5}S_{10}A_{0.5}$, $C_{88}S_{10}A_1$, and $C_{88}S_{10}A_2$, respectively. The rate of strength gain from 14 to 28 days increased by 237.53, 70.14, and 194.6 % in $C_{90}S_{10}A_0$, $C_{89}S_{10}A_1$ and $C_{88.5}S_{10}A_{1.5}$, and decreased by 81.43, 29.81 and 16.61 % in $C_{99.5}S_0A_{0.5}$, $C_{89.5}S_{10}A_{0.5}$ and $C_{88}S_{10}A_2$, respectively, in comparison with $C_{100}S_0A_0$.

This implies that ASW contributes to the strength development through their attachment with free silica to form aluminosilicate products. This aluminosilicate network contributes to the skeletal framework to induce strength gain as indicated in Fig. 9. Moreover, the portlandite that ought to react with SF to produce additional CSH was consumed by ASW (Eqs. (1), (3)) thereby leading to the evolution of hydrogen that caused the reduction in the unit weight of the samples as shown in Fig. 7.

$$CS + H \rightarrow CSH + CH. \tag{3}$$

The ASW-SF blended OPC mortar ($C_{89}S_{10}A_1$) performs better than SF blended mortar ($C_{90}S_{10}A_0$). The optimum quantity to foster performance in ASW-SF blended mortar is 1%, since the Sulphate/Al ratio plays a key role in the formation of aluminoferrite mono-sulphate (Afm), unlike low density Aft with pore filling characteristics, which can improve the compressive strength [28]. Afm has greater density due to increase in Sulfate/ASW ratio at lower substitution up to 0.5 %, that can cause weak microstructure. Lower sulfate/ASW ratio could also lead to lower compressive strength due to more porosity that accompanies the evolution of hydrogen gas within the matrix. This explains the reason why $C_{88.50}S_{10}A_{1.5}$ and $C_{88.50}S_{10}A_2$ have lower strengths in comparison with $C_{89}S_{10}A_1$. The presence of ASW reduces the dilution effect of SF during pozzolanic reaction in mortar production.

XRD in Fig. 10 shows the possible formation of mayenite ($Ca_{12}Al_{14}O_{33}$), ettringite and muscovite ($K_2(Al_2O_3)_3(SiO_2)_6H_2O$), which further justify the possibility of Eq. 1. The dual presence of ettringite and mayenite due to reaction of ASW with gypsum and other cement compounds could be responsible for the decrease in the compressive strength in comparison with $C_{100}S_0A_0$ and $C_{89}S_{10}A_0$. It also shows that the presence of ASW does not prevent the formation of calcium silicate hydrate (CSH) and portlandite ($Ca(OH)_2$) as clearly shown in Fig. 10, while the presence of C_4AF, alite (C_3S) and belite (C_2S) could be

due to the presence of unreacted cement within the matrix. The removal of hydrogen gas led to more microstructural voids that induced carbonation thereby leading to the formation of calcium carbonate or calcite ($CaCO_3$).

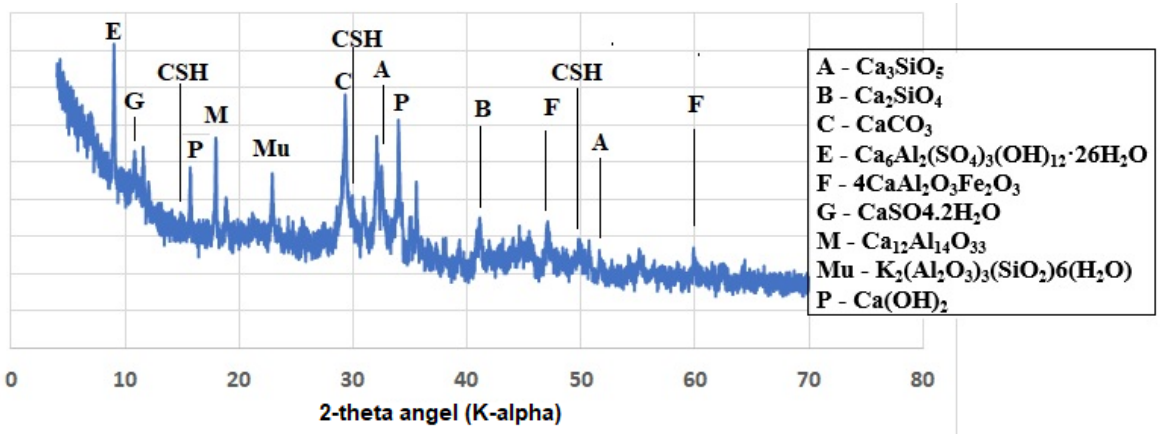

Figure 10. X-ray diffractogram of the SF-ASW ternary blended paste.

Fig. 11 shows the Fourier transform infrared (FTIR) spectroscopy and indicates asymmetric stretching of Al-O bond and Al_2O_3 vibration at 1119 cm^{-1} and 997 cm^{-1}, respectively, while wavenumber 874 cm^{-1} indicates C-O vibration from the carbonate source. Besides, C-O vibration due to carbonation (region B) is indicated in the wavenumber 2336 cm^{-1} [18, 29]. Similarly, region A and C point to OH and HOH vibration were due to the presence of portlandite. The presence of ASW does not appear to affect the C-O band at 1420 cm^{-1}, but in contrast, it has significant impact on Si-OH and HOH bending mode vibration in water at 1638 cm^{-1} due to interaction with tricalcium aluminate (C_3A) to form aluminosilicate bonds [30]. The calcium aluminate phase has been assigned by Tarte [26] to the wavenumber with 700–900 cm^{-1} for condensed aluminate $CaO.Al_2O_3$, $12CaO.7Al_2O_3$ and theta-Al_2O_3, which was further supported by Yusuf [29], and Fernendez-Carrasco et al. [25, 29].

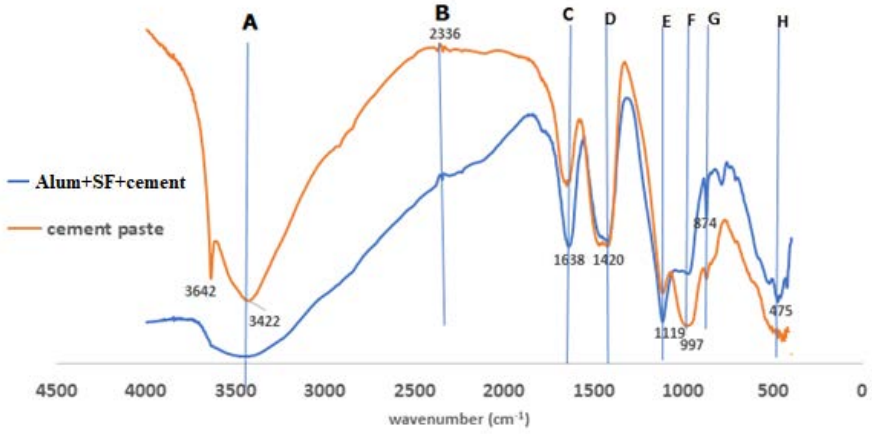

Figure 11. FTIR of ASW blended paste in comparison with OPC cement paste.

The isolated and condensed octahedral AlO_4 were identified at wavenumber 650–800 and 530–400 cm^{-1}, respectively [26]. Therefore, the peak at point G in Fig. 11 can be said to be due to the presence of calcium aluminate hydroxide (CAH). Besides, the OH/HOH vibration was noted at 3422 cm^{-1} while the absence of ASW in the control sample (hydrated cement) led to the presence of OH peaks at 3642 cm^{-1}, which was absent in ASW blended mortar.

3.5. Thermal residual strength of ASW-SF blended mortar

By comparing 28-day strength, addition of ASW into OPC mortar caused reduction in compressive strength at room temperature (Fig. 12). There is a decrease in the residual thermal strength in OPC due to microstructural disintegration as the thermal residual 28-day strength was 37 % less than that at room temperature. However, under thermal treatment (300 °C for 1 h), addition of 0.5, 1, 1.5 and 2 % ASW caused increase in strength by 18.5, 29.2, 2.4, 11 and 26.2 % in comparison with $C_{100}S_0A_0$ as noted in $C_{99.5}S_0A_{0.5}$, $C_{89.5}S_{10}A_{0.5}$, $C_{89}S_{10}A_1$, $C_{88.5}S_{10}A_{1.5}$, and $C_{88}S_{10}A_2$, respectively. Both SF and ASW have positive

impacts on thermal treatment by incorporating 0.5, 1, 1.5 and 2 % ASW, through the achievement of positive strength gains of 39.8, 43.5, 61, 50.4 and 29.7 %, respectively.

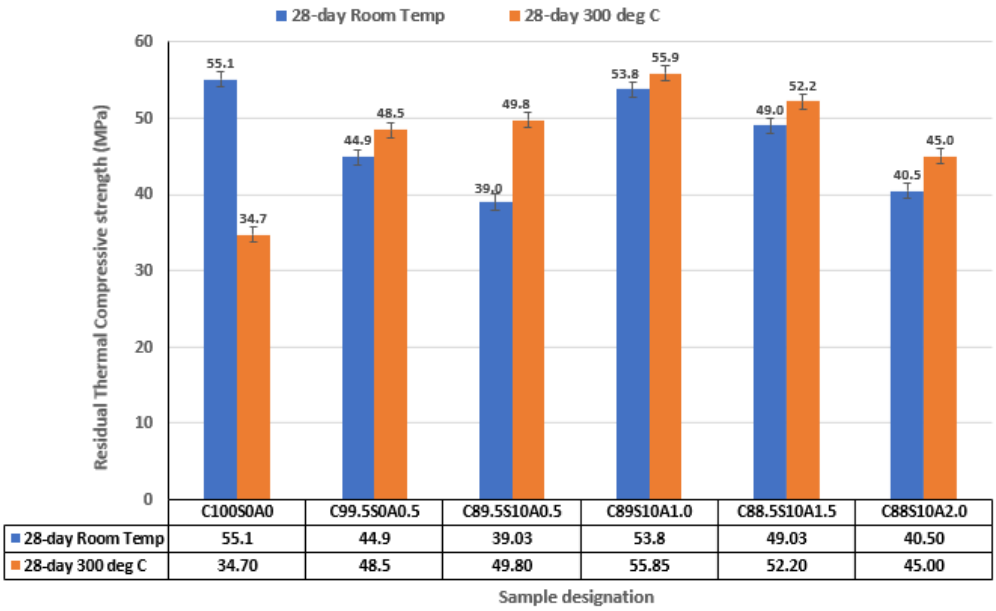

Figure 12. Compressive strength of alumina blended mortar.

Inclusion of ASW contributed significantly to the thermal residual strength as compressive strength by 8, 27.6, 3.8, 3.5 and 11.1 % in $C_{99.5}S_0A_{0.5}$, $C_{89.5}$ $S_{10}A_{0.5}$, $C_{89}S_{10}A_1$, $C_{88.5}$ $S_{10}A_{1.5}$, and $C_{88}S_{10}A_2$, respectively. There is no observable physical deterioration in any of the samples. Therefore, the optimum thermal performance was observed when the ASW inclusion is 0.5 % in the presence of SF ($C_{89.5}S_{10}A_{0.5}$) even though the maximum thermal strength was obtained with 1 % ASW. This indicates that the presence of ASW+SF improves thermal performance due to attachment of Si to Al in tetrahedral coordination to induce the formation of zeolite-like product (CASH) as observable in geopolymer synthesis [31–33].

3.6. Microstructure and elemental ratio of ASW-SF blended paste

Fig. 13 shows the contribution of ASW to the microstructural morphology and the elemental compositions of the product formed. The region 1 and 3 indicate that the general spectrum of ASW-Si blended paste was such that Ca/Si ratio was 1.83 and 2.9, respectively, while the region 4 at which Aft or ettringite was formed had the Ca/Si ratio of 3.34. At the region 2 where the bubbles formed, the Ca/Si ratio decreases to 0.76. The low Ca/Si ratio in this region causes a decrease in the compressive strength recorded when compared to SF-ASW based samples. Calcium to carbon (Ca/C) ratios are 1.25 and 1.68 at regions 1 and 3 while the region 4 (where Aft formed) had 1.40. The presence of graphite in ASW as noticed in the XRD in Fig. 2 was supported by the presence of carbon in the energy dispersion spectroscopy (EDS) (Fig.13). The presence of a bubble could make the matrix susceptible to carbonation thereby causing Ca/C to be 0.76 (region 2). The presence of Fe in region 1 pointed to the possibility of unreacted cement powder that contained tetracalcium aluminoferrite (F-C_4AF) as shown in the XRD in OPC raw powder (Fig. 2).

4. Conclusions

This paper investigates the impact of the synergy of silica fume (SF) and aluminium shaving waste (ASW) on the strength and thermal performance of ternary blended mortar comprising ordinary Portland cement, aluminium shaving waste powder and silica fume (OPC+ASW+SF). The following conclusions can be drawn:

1. Silica fume reduced the workability of mortar and concrete whereas the use of ASW enhanced the consistency of the binder by up to 32 % at the level of 0.5–2 % without compromising the strength significantly.

2. ASW enhanced the formation of calcium aluminate hydrate (CAH) together with calcium silicate hydrate (CSH). This is established by the presence of mayenite and muscovite among the peaks identified by X-ray diffractogram.

3. Thermal exposure of ASW-SF sample to 300 °C for 1 hr significantly reduced the unit weight of the samples by 12.03, 4.16 and 4.27 % for 0.5, 1 and 1.5 %, respectively while 2 % ASW led to an increase

in the unit weight of the sample by 4.4 %. It implies that 0.5 % ASW had the most significant effect on the density of the sample.

4. The strength gain in 10%SF-0.5%ASW and 0%SF-0.5%ASW blended mortar exposed to 300 °C for 1 hr were 8 % and 26 % when compared to those produced at room temperature. Exposing ordinary Portland cement (OPC) to similar condition led to 37 % decrease in strength compared to those prepared at room temperature.

5. The optimal 28-day strength performance of the mortar of 53.8 MPa was obtained in the sample produced with 10%SF, 1 % ASW and 89 % OPC. There was 3.9 % gain in strength when the samples were exposed to 300 °C for 1 hr.

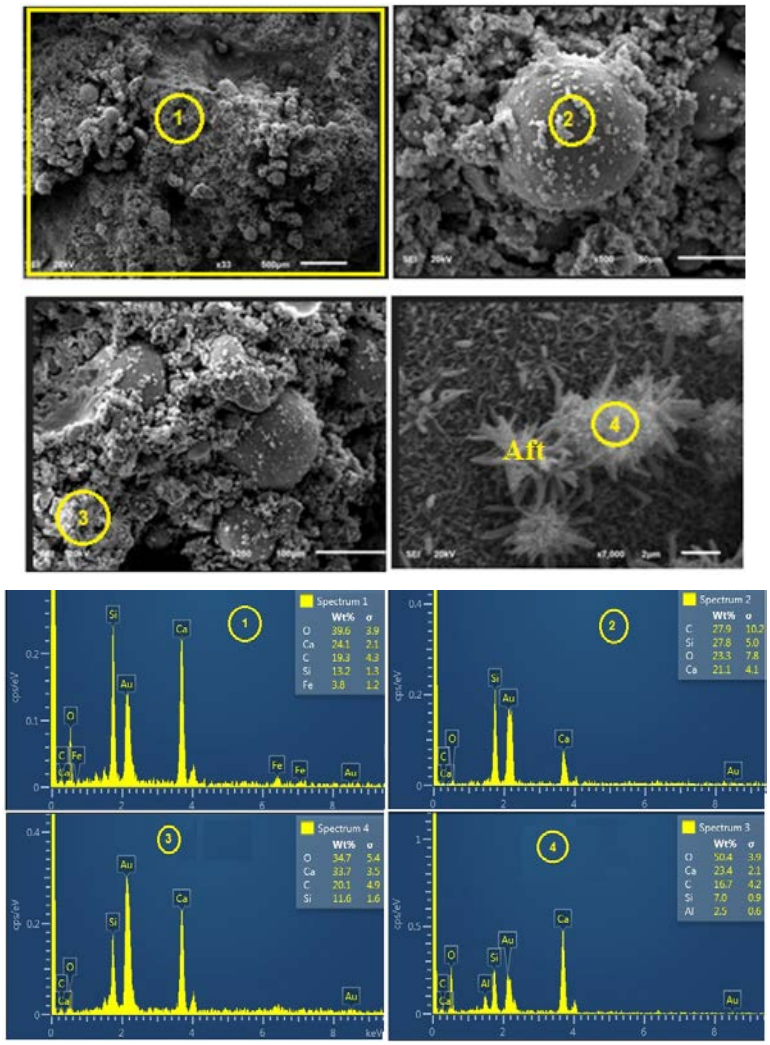

Figure 13. Morphology of SF-ASW blended mortar.

References

1. Gerbelova, H., Spek, M.V., Schakel, W. Feasibility assessment of CO_2 capture retrofitted to an existing cement plant: post-combustion vs. Oxy-fuel combustion technology. Energy Procedia. 2017. 114. Pp. 6141–6149. DOI: 10.1016/j.egypro.2017.03.1751
2. Ungureanu, C.A., Das, S.K., Jawahir, I.S. Life-cycle cost analysis: aluminum versus steel in passenger cars. Aluminum Alloys for Transportation, Packaging, Aerospace, and Other Applications. 2007. Pp. 11–24.
3. Sabapathy, Y.K., Sabarish, S., Nithish, C.N.A, Ramasamy, M., Krishna, G. Experimental study on strength properties of aluminium fibre reinforced concrete. Journal of King Saud University – Engineering Sciences. 2021. 33(1). Pp. 23–29. DOI: 10.1016/j.jksues.2019.12.004
4. Ofuyatan, O. et al., Effect of waste aluminium shavings on the bond characteristics of laterized concrete. Advances in Materials Research. 2019. 8(1). Pp. 25–36. DOI: 10.12989/amr.2019.8.1.025
5. Gulmez, N. Reuse of industrial metal wastes as partial replacement of aggregates in mortar production, DÜMF Mühendislik Dergisi. 2021. Pp. 875–880. DOI: 10.24012/dumf.1051502
6. Tang, V.L., Vu, K.D., Ngo, X.H., Vu, D.T., Bulgakov, B., Bazhenova, S. Effect of Aluminium Powder on Light-weight Aerated Concrete Properties. E3S Web of Conferences. 2019. 97. DOI: 10.1051/e3sconf/20199702005

7. Kinoshita, H. et al. Corrosion of aluminium metal in OPC- and CAC-based cement matrices. Cement and Concrete Research. 2013. 50. Pp. 11–18. DOI: 10.1016/j.cemconres.2013.03.016
8. Shabbar, R., Nedwell, P., Wu, Z. Mechanical properties of lightweight aerated concrete with different aluminium powder content, in MATEC Web of Conferences. 2017. 120. DOI: 10.1051/matecconf/201712002010
9. Moghaddam, H.H., Lotfollahi-Yaghin, M.A., Maleki, A. Durability and mechanical properties of self-compacting concretes with combined use of aluminium oxide nanoparticles and glass fiber, International Journal of Engineering, Transactions A: Basics. 2021. 34(1). Pp. 26–38. DOI: 10.5829/IJE.2021.34.01A.04
10. Kuziak, J., Zalegowski, K. Jackiewicz-Rek, W., Stanisławek, E. Influence of the type of cement on the action of the admixture containing aluminum powder. Materials. 2021. 14(11). DOI: 10.3390/ma14112927
11. Shabbar, R., Nedwell, P., Al-Taee, M., Wu, Z. Effect of Different Aluminium Powder Content on the Behaviour of Aerated Concrete: Experimental and Finite Element Validation, International Journal of Materials, Mechanics and Manufacturing. 2018. 6(2). Pp. 155–158. DOI: 10.18178/ijmmm.2018.6.2.367
12. Ramamurthy, K., Narayanan, K. Factors influencing the density and compressive strength of aerated concrete. Magazine of Concrete Research. 2000. 52(3). Pp. 163–168. DOI: 10.1680/macr.2000.52.3.163
13. Muthu Kumar, E., Ramamurthy, K. Effect of fineness and dosage of aluminium powder on the properties of moist-cured aerated concrete. Constr Build Mater. 2015. 95. Pp. 486–496. DOI: 10.1016/j.conbuildmat.2015.07.122
14. Guglielmi, P.O., Silva, W.R.L., Repette, W.L., Hotza, D. Porosity and mechanical strength of an autoclaved clayey cellular concrete. Advances in Civil Engineering. 2010. 7. DOI: 10.1155/2010/194102
15. Narayanan, N., Ramamurthy, K. Structure and properties of aerated concrete: A review. Cement and Concrete Composites. 2000. 22(5). Pp. 321–329. DOI: 10.1016/S0958-9465(00)00016-0
16. Elinwa, A.U., Mbadike, E. The use of Aluminum waste for concrete production. Journal of Asian Architecture and Building Engineering. 2011. 10(1). Pp. 217–220. DOI: 10.3130/jaabe.10.217
17. Azarhomayun, F., Haji, M., Kioumarsi, M., Shekarchi, M. Effect of calcium stearate and aluminum powder on free and restrained drying shrinkage, crack characteristic and mechanical properties of concrete. Cement and Concrete Composites. 2022. 125. 104276. DOI: 10.1016/j.cemconcomp.2021.104276
18. Herting, G., Odnevall, I. Corrosion of Aluminium and Zinc in Concrete at Simulated Conditions of the Repository of Low Active Waste in Sweden. Corrosion and Materials Degradation. 2021. 2(2). Pp. 150–163. DOI: 10.3390/cmd2020009
19. Faez, A., Sayari, A., Manie, S. Mechanical and Rheological Properties of Self-Compacting Concrete Containing Al_2O_3 Nanoparticles and Silica Fume, Iranian Journal of Science and Technology - Transactions of Civil Engineering. 2015. 44. Pp. 217–227. DOI: 10.1007/s40996-019-00339-y
20. ASTM C150-07, Standard Specification for Portland Cement. ASTM International, 2007.
21. ASTM C157, Standard Test Method for Length Change of Hardened Hydraulic-Cement Mortar and Concrete, 2008.
22. ASTM C1437-20, Standard Test Method for Flow of Hydraulic Cement Mortar. ASTM International, 2020.
23. ASTM C109/C109M-20, Standard Test Method for Compressive Strength of Hydraulic Cement Mortars (Using 2-in. or [50-mm] Cube Specimens). ASTM International, 2020.
24. Morterra, C., Magnacca, G. A case study: surface chemistry and surface structure of catalytic aluminas, as studied by vibrational spectroscopy of adsorbed species. Catal Today. 1996. 27(3–4). Pp. 497–532. DOI: 10.1016/0920-5861(95)00163-8
25. Fernández-Carrasco, L. Torrens-Martín, D. Morales, L.M, Martínez-Ramírez, S. Infrared Spectroscopy in the Analysis of Building and Construction Materials. Infrared Spectroscopy – Materials Science, Engineering and Technology. Prof. Theophanides Theophile, Ed. 5100 Rijeka Croatia: Tech, 2012. Pp. 369–381. DOI: 10.5772/36186
26. Tarte, P. Infra-red spectra of inorganic aluminates and characteristic vibrational frequencies of AlO_4 tetrahedra and AlO_6 octahedra. Spectrochim Acta A. 1967. 23(7). Pp. 2127–2143. DOI: 10.1016/0584-8539(67)80100-4
27. Studart, A.R., Innocentini, M.D.M., Oliveira, I.R., Pandolfelli, V.C. Reaction of aluminum powder with water in cement-containing refractory castables. Journal of the European Ceramic Society. 2005. 25(13). Pp. 3135–3143. DOI: 10.1016/j.jeurceramsoc.2004.07.004.
28. Hartman, M.R., Berliner, R. Investigation of the structure of ettringite by time-of-flight neutron powder diffraction techniques. Cement and Concrete Research. 2006. 36(2). Pp. 364–370. DOI: 10.1016/j.cemconres.2005.08.004
29. Yusuf, M.O. Bond Characterization in Cementitious Material Binders Using Fourier-Transform Infrared Spectroscopy. Applied Sciences. 2023. 13(5). Pp. 3353. DOI: 10.3390/app13053353
30. Gatta, G.D., Hålenius, U., Bosi, F., Cañadillas-Delgado, L., Fernandez-Diaz, M.T. Minerals in cement chemistry: A single-crystal neutron diffraction study of ettringite, $Ca_6Al_2(SO_4)_3(OH)_{12}{\cdot}27H_2O$. American Mineralogist. 2019. 104(1). Pp. 73–78. DOI: 10.2138/am-2019-6783
31. Yusuf, M.O., Megat Johari, M.A., Ahmad, Z.A., Maslehuddin, M. Effects of addition of $Al(OH)_3$ on the strength of alkaline activated ground blast furnace slag-ultrafine palm oil fuel ash (AAGU) based binder. Construction and Building Materials. 2014. 50. Pp. 361–367. DOI: 10.1016/j.conbuildmat.2013.09.054
32. Fernández-Jiménez A and Palomo, A. Composition and microstructure of alkali activated fly ash binder: Effect of the activator. Cement and Concrete Research. 2005. 35(10). Pp. 1984–1992. DOI: 10.1016/j.cemconres.2005.03.003
33. Alonso, S., Palomo, A. Alkaline activation of metakaolin and calcium hydroxide mixtures: influence of temperature, activator concentration and solids ratio. Materials Letters. 2001. 47(1-2). Pp. 55–62. DOI: 10.1016/S0167-577X(00)00212-3

Information about authors:

Moruf O. Yusuf, *PhD*
ORCID: https://orcid.org/0000-0002-8134-5435
E-mail: moruf@uhb.edu.sa
E-mail: moruff@gmail.com

Received 03.05.2023. Approved after reviewing 08.08.2023. Accepted .14.08.2023